Computers and Concrete, *Vol. 20, No. 1 (2017) 85-97*
DOI: https://doi.org/10.12989/cac.2017.20.1.085

A physically consistent stress-strain model for actively confined concrete

Sharif Shahbeyk*, Mahshid Z. Moghaddam[a] and Mohammad Safarnejad[b]

Faculty of Civil and Environmental Engineering, Tarbiat Modares University, Jalal Ale Ahmad Highway, P.O. Box 14115-143, Tehran, Iran

(Received June 21, 2016, Revised March 22, 2017, Accepted March 23, 2017)

Abstract. With a special attention to the different stages of a typical loading path travelled in a fluid confined concrete test, this paper introduces a physically consistent model for the stress-strain curve of actively confined normal-strength concrete in the axial direction. The model comprises of the five elements of: (1) a criterion for the peak or failure strength, (2) an equation for the peak strain, (3) a backbone hydrostatic curve, (4) a transient hardening curve linking the point of departure from the hydrostatic curve to the failure point, and finally (5) a set of formulas for the post-peak region. Alongside, relevant details and shortcomings of existing models will be discussed in each part. Finally, the accuracy and efficiency of the proposed model have been verified in a set of simulations which compare well with the experimental results from the literature.

Keywords: active confinement; concrete; failure strength; stress-strain model; hydrostatic response; numerical modeling

1. Introduction

Axial compressive behavior of confined concrete has received significant attention over the last decades as confinement enhances the load carrying capacity of concrete and improves its ductility, features of crucial importance especially for structural members subjected to severe loads. Depending on how confining stresses are provided and applied to specimens, concrete failure studies are categorized as being active or passive. Confinement exerted by fluid applying hydrostatic pressure on a concrete core is of active type. On the other hand, fiber-reinforced polymer (FRP) jackets and lateral reinforcements such as spirals or ties provide passive confinement activated by the expansion of concrete. Recently, shape memory alloys (SMA) have also been used as confining materials which can provide a combination of active and passive confinements.

Actively confined concrete studies are of great significance as their importance is multifold: first, the results of such research can directly provide grounds for more realistic modeling of actively confined structural members (e.g., pressure vessels), second, they indirectly play an essential role in the accuracy of the existing analysis-oriented models for passively confined concrete as, in almost all of these models, each point on the stress-strain curve of passively confined concrete corresponds to a point on an actively confined curve with the same confining stress as exerted by the confining material (see e.g., Spoelstra and Monti 1999, Harries and Kharel 2002, Marques *et al.* 2004, Albanesi *et al.* 2007, Jiang and Teng 2007, Teng *et al.* 2007, Xiao *et al.* 2010, and Ghorbi *et al.* 2013 for FRP confined cylinders, the work of Shin and Andrawes 2010 on SMA confined concrete, and the review article of Ozbakkaloglu *et al.* (2013) for complementary information), and third, the accuracy of the numerical simulations employing directly or indirectly these analysis-oriented models (see e.g., Montuori *et al.* 2013, Ding *et al.* 2017, and Sadeghi and Nouban 2017) depends on the extent the underlying actively confined models are loyal to the real response of concrete.

The first actively confined model may be attributed to Mander *et al.* (1988). Improved versions of this model were employed in Samdani and Sheikh (2005), Marques *et al.* (2004), Teng *et al.* (2007), Jiang and Teng (2007), and Xiao *et al.* (2010). Moreover, other actively confined models were suggested by Attard and Setunge (1996), Harries and Kharel (2002), Binici (2005), and Samani and Attard (2012) whose structures differ from that of Mander *et al.* (1988). These existing models and especially the ones proposed in recent years were shown to be rather successful in the prediction of stress-strain curves of actively confined concrete, however, as will be shown and discussed in this study, situations arise in which physically incorrect predictions are obtained. The reason behind these kinds of inadequateness is that most of the existing models have been phenomenologically developed without enough attention to the loading path travelled in an actual fluid confined test.

Motivated by the observed inconsistencies and inaccuracies, the current study proposes a new stress-strain model for actively confined concrete which is closely loyal to the process of loading in fluid confined concrete tests. Accordingly, the stress path is divided into two phases initiated by a hydrostatic part up to the predefined confining stress provided by the fluid, f_l, and, continued by a triaxial part in which the confining pressure is kept constant and equal to f_l. Alongside, existing relations for the peak stress, peak strain, and post-peak region of actively confined normal-strength concrete (NSC) are carefully re-evaluated

*Corresponding author, Assistant Professor
E-mail: shahbeyk@modares.ac.ir
[a]M.Sc.
[b]Ph.D.

http://www.techno-press.org/?journal=cac&subpage=8
ISSN: 1598-8198 (Print), 1598-818X (Online)

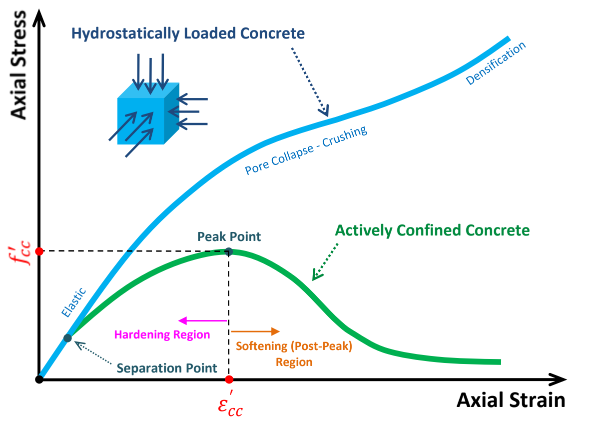

Fig. 1 Stress-strain curves of hydrostatically loaded and actively confined concrete samples

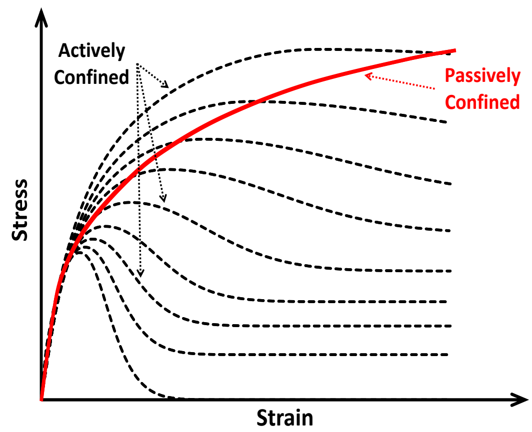

Fig. 2 Simulation of a stress-strain curve of passively confined concrete using an analysis-oriented model

against experimental results from the literature and a set of more conforming formulas have been suggested. An equation for the transient hardening part of the stress-strain curve is also proposed which links the point of departure from the hydrostatic curve to the failure point. Finally, comparisons are made between the predictions of proposed model and available test results.

2. Actively confined concrete

2.1 Introductory remarks

The stress-strain curve of a hydrostatically loaded concrete sample and that of a typical actively confined concrete specimen are shown in Fig. 1. The hydrostatic stress-strain curve of normal concrete consists of the three elastic, pore collapse, and densification phases. On the other hand, an actively confined test begins with a gradual increase of triaxial hydrostatic pressure up to a predefined value (first phase of loading) and then, keeping constant the applied confining pressure, is followed with an extra uniaxial load (second phase of loading). As illustrated in Fig. 1, in contrary to a pure hydrostatic test, the stress-strain curve of actively confined concrete experiences a global maximum known as its peak point and thus can be divided into two distinct hardening and softening (post-peak) parts.

Up to now, many researchers have tried to propose appropriate models for the prediction of stress-strain curve of actively confined concrete (see, e.g., Mander *et al.* 1988, Attard and Setunge 1996, Harries and Kharel 2002, Marques *et al.* 2004, Binici 2005, Samdani and Sheikh 2005, Jiang and Teng 2007, Teng *et al.* 2007, and Samani and Attard 2012). It needs to note that the main importance of such models should be sought elsewhere, first in their applications in the development of analysis-oriented models for passively confined concrete in which each point on the stress-strain curve corresponds to a point on an actively confined curve with the same confining stress as exerted by the confining material (Fig. 2), and second when they play the role of constitutive laws for finite element integration points, in fiber-type beam-column models, or in other computational frameworks. Accordingly, if incorrect hypotheses are postulated in an actively confined concrete model, inaccurate or even physically irrelevant results may be immediately appeared in the predictions of the corresponding analysis-oriented or numerical model.

2.2 An overview of the existing actively confined concrete models

The introduction of first actively confined model can be attributed to Mander *et al.* (1988) who proposed a stress-strain relationship of the following form

$$f_{cc} = \frac{xr}{r-1+x^r} f'_{cc}$$
$$x = \frac{\varepsilon_{cc}}{\varepsilon'_{cc}}, \qquad r = \frac{E_c}{E_c - E_{sec}}, \qquad E_{sec} = \frac{f'_{cc}}{\varepsilon'_{cc}} \tag{1}$$

f'_{cc} and ε'_{cc} are the peak strength and peak strain of confined concrete, respectively, and E_c is the concrete elastic modulus. Following their work, Spoelstra and Monti (1999), Fam and Rizkalla (2001), and Albanesi *et al.* (2007) used the very same formulas of Mander *et al.* (1988) and put forward their models for passively confined concrete. Moreover, there exist some other analysis-oriented models such as those of Marques *et al.* (2004), Samdani and Sheikh (2005), Jiang and Teng (2007), Teng *et al.* (2007), and Xiao *et al.* (2010) in which Eq. (1) was used for their stress-strain curves yet with modified peak strain/peak strength formulas. Besides, Attard and Setunge (1996), Harries and Kharel (2002), Binici (2005), and Samani and Attard (2012) incorporated their own equations and proposed alternative actively confined concrete models. Details of all these models are provided in Table 1. In this table and hereinafter, ϕ, ψ, and χ are the confinement ratio (confining strength divided by concrete uniaxial compressive strength, f'_c), the peak strength ratio, (compressive strength of confined concrete divided by f'_c), and the peak strain ratio, (peak compressive strain of confined concrete divided by that of uniaxial compression, ε'_c), respectively.

2.3 Elastic response of the models

Before proceeding to the structure of our proposed

Table 1 Some of the formulas for the stress-strain curve of actively confined concrete

Model	Stress-Strain Formula ($f_{cc} - \varepsilon_{cc}$)	Peak Strength Ratio (ψ)	Peak Strain Ratio (χ)
Mander *et al.* (1988)	$f_{cc} = \frac{xr}{r-1+x^r} f'_{cc}$	$2.254\sqrt{1+7.94\phi} - 2\phi - 1.254$	$5\psi - 4$
Attard and Setunge (1996)	$f_{cc} = \frac{Ax+Bx^2}{1+(A-2)x+(B+1)x^2} f'_{cc}, \quad 0 \le x \le 1, \quad 0 \le f_{cc} \le f'_{cc}$ $A = \frac{E_c \varepsilon'_{cc}}{f'_{cc}} \qquad B = \frac{(A-1)^2}{0.55} - 1$	$\left(\frac{f_l}{f_t} + 1\right)^k$ $k = 1.25(1+0.062\phi){f'_c}^{-0.21}$	$1 + (17 - 0.06f'_c)\phi$
Harries and Kharel (2002)	$f_{cc} = \frac{xr}{r-1+x^{kr}} f'_{cc}, \quad \begin{cases} k = 1 & x \le 1 \\ k = \left(0.67 + \frac{f'_c}{62}\right)\frac{f'_c}{f'_{cc}} \ge 1 & x > 1 \end{cases}$	$2.254\sqrt{1+7.94\phi} - 2\phi - 1.254$	$5\psi - 4$
Marques *et al.* (2004)	$f_{cc} = \frac{xr}{r-1+x^r} f'_{cc}$	$1 + k_1\phi$ $k_1 = 6.7f_l^{-0.17}$	$1 + 5k_1k_3\phi, \quad \begin{cases} k_1 = 6.7f_l^{-0.17} \\ k_3 = \frac{40}{f'_c} \le 1 \end{cases}$
Binici (2005)	$f_{cc} = \begin{cases} E_c\varepsilon_{cc} & \varepsilon_{cc} \le \varepsilon_{ce} \\ f_{ce} + (f'_{cc} - f_{ce})\left(\frac{\varepsilon_{cc} - \varepsilon_{ce}}{\varepsilon'_{cc} - \varepsilon_{ce}}\right)\frac{r}{r-1+\left(\frac{\varepsilon_{cc}-\varepsilon_{ce}}{\varepsilon'_{cc}-\varepsilon_{ce}}\right)^r} & \varepsilon_{ce} < \varepsilon_{cc} \le \varepsilon'_{cc} \\ f_{cr} + (f'_{cc} - f_{cr})\exp\left[-\left(\frac{\varepsilon_{cc}-\varepsilon'_{cc}}{\alpha}\right)^2\right] & \varepsilon_{cc} > \varepsilon'_{cc} \end{cases}$ $r = \frac{E_c}{E_c - \frac{f'_{cc} - f_{ce}}{\varepsilon'_{cc} - \varepsilon_{ce}}}, \qquad \alpha = \frac{1}{\sqrt{\pi}(f'_{cc} - f_{cr})}\left(\frac{2G_{fc}}{l_c} - \frac{(f'_{cc} - f_{cr})^2}{E_c}\right)$	$\psi = \phi + \sqrt{1+9.9\phi}$	$5\psi - 4$
Samdani and Sheikh (2005)	$f_{cc} = \frac{xr}{r-1+x^r} f'_{cc}$	$1 + 6.42\frac{f_l^{0.9}}{f'_c}$	$5\psi - 4$
Teng *et al.* (2007)	$f_{cc} = \frac{xr}{r-1+x^r} f'_{cc}$	$1 + 3.5\phi$	$1 + 17.5\phi$
Jiang and Teng (2007)	$f_{cc} = \frac{xr}{r-1+x^r} f'_{cc}$	$1 + 3.5\phi$	$1 + 17.5\phi^{1.2}$
Xiao *et al.* (2010)	$f_{cc} = \frac{xr}{r-1+x^r} f'_{cc}$	$\begin{cases} 1 + 3.34\phi^{0.79} & \text{HSC} \\ 1 + 3.24\phi^{0.80} & \text{HSC and NSC} \end{cases}$	$\begin{cases} 1 + 18.8\phi^{1.10} & \text{HSC} \\ 1 + 17.4\phi^{1.06} & \text{HSC and NSC} \end{cases}$
Samani and Attard (2012)	$f_{cc} = \frac{Ax+Bx^2}{1+(A-2)x+(B+1)x^2} f'_{cc}, \quad 0 \le x \le 1, \quad 0 \le f_{cc} \le f'_{cc}$ $A = \frac{E_c \varepsilon'_{cc}}{f'_{cc}} \qquad B = \frac{(A-1)^2}{0.55} - 1$	$\left(\frac{f_l}{f_t} + 1\right)^k$ $k = 1.25(1+0.062\phi){f'_c}^{-0.21}$	$\exp(k)$ $k = (2.9224 - 0.00367f'_c)\phi^{0.3124+0.002f'_c}$

Table 2 Initial elastic slopes predicted by the existing actively confined stress-strain models

Model	$\frac{\mathrm{d}f_{cc}}{\mathrm{d}\varepsilon_{cc}}$	$E_{cc} = \left.\frac{\mathrm{d}f_{cc}}{\mathrm{d}\varepsilon_{cc}}\right\rvert_{\varepsilon_{cc}=0}$
Attard and Setunge (1996), Samani and Attard (2012)	$\left\{\frac{2Bx+A}{1+(A-2)x+(B+1)x^2} - \frac{(Bx^2+Ax)[A-2+2(B+1)x]}{[1+(A-2)x+(B+1)x^2]^2}\right\}\frac{f'_{cc}}{\varepsilon'_{cc}}$	E_c
Mander *et al.* (1988), Spoelstra and Monti (1999), Fam and Rizkalla (2001), Harries and Kharel (2002), Marques *et al.* (2004), Binici (2005), Samdani and Sheikh (2005), Albanesi *et al.* (2007), Jiang and Teng (2007), Teng *et al.* (2007), Xiao *et al.* (2010)	$\left[\frac{r}{r-1+x^r} - \frac{r^2x^r}{(r-1+x^r)^2}\right]\frac{f'_{cc}}{\varepsilon'_{cc}}$	E_c

model in the next section, it is worth noting that all of the existing actively confined concrete models ignored this fact that the stress-strain curve should match the hydrostatic response in the initial phase of loading. To check one of the consequence of this simplification, let's examine the initial elastic response predicted by the models of Table 1 for the hydrostatic loading case. From the mechanics of materials, the slope of elastic part of a hydrostatic curve, E_{cc}, is equal to

$$E_{cc} = \left.\frac{\mathrm{d}f_{cc}}{\mathrm{d}\varepsilon_{cc}}\right|_{\varepsilon_{cc}=0} = \frac{1}{1-2\nu}E_c \tag{2}$$

where ν is the elastic Poisson's ratio of concrete. However, as presented in Table 2, all of the elastic slopes predicted by the models for the hydrostatic loading case are mistakenly equal to the Young modulus, E_c. This shortcoming exists for other triaxial loading cases and directly affects the accuracy of emanating analysis-oriented models for passively confined concrete. Now, one can interpret why Montuori *et al.* (2012) identified cases for which the constitutive laws of FRP confined concrete provided initial slopes less than those obtained for the same sections with reference to the model of unconfined concrete. This fact may be downplayed by some of the researchers focusing on the ultimate strength of confined concrete, however, when it comes to the application of such analysis-oriented models in a numerical frameworks (e.g., in the finite or applied element methods), the very early requirement is that their macro and micro elastic predictions should be correct, the fact cannot be granted by the existing actively confined concrete models.

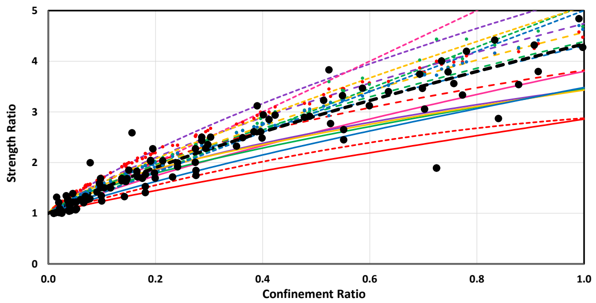

(a)

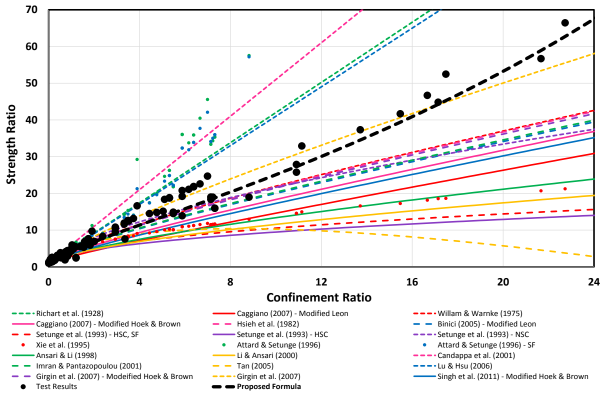

(b)

Fig. 3 Predictions of the models for the strength ratio. (a) Low-confinement ratios and (b) all confinement ratios

3. Elements of the proposed model

In analogy to the typical form of actively confined concrete stress-strain curve shown in Fig. 1, the model proposed in this study is made up of: (1) a criterion defining peak strength, (2) an equation for the failure strain, (3) a backbone hydrostatic curve to define the initial loading phase, (4) a transient hardening part linking the point of departure from the hydrostatic curve to the failure point, and finally (5) a set of formulas for the post-peak region. These five elements of the model would be separately discussed in the following subsections. Alongside, relevant weaknesses and strengths of the existing models would be discussed in each part.

3.1 Peak strength criterion

Numerous experiments have been carried out on fluid-confined NSC. The first well-known study of this type was conducted by Richart *et al.* (1928). Since then, Chinn and Zimmerman (1965), Kotsovos and Newman (1978), Smith *et al.* (1989), Lahlou *et al.* (1992), Hansen (1995), Imran and Pantazopoulou (1996), Ansari and Li (1998), Candappa *et al.* (2001), Sfer *et al.* (2002), Laine (2004), Tan (2005), Gabet *et al.* (2008), Dupray *et al.* (2009), and Vu *et al.* (2009) have performed comprehensive experiments on NSC with confinement ratios up to 3.9, 17.1, 1.5, 0.4, 0.5, 0.15, 1, 0.9, 0.3, 1.8, 0.4, 1.2, 16.7, 22.7, 21.7, and 5, respectively. For ease of discussion, the confinement ratios are classified in this study into two ranges of: (1) low-confinement ratios corresponding to $\phi \leq 1$ and (2) high-confinement ratios defined by $\phi > 1$.

A database containing the results of axial compressive tests on actively confined NSC cylinders is employed herein to assess the performance of the existing strength criteria. It contains the test results of more than 160 actively confined concrete specimens gathered from the literature which includes 108 and 56 concrete specimens tested under low and high-confinement ratios, respectively. Figs. 3(a)-3(b) show the peak compressive strength ratio versus ϕ for the samples tested under low-confinement ratios and the whole database, respectively.

Many researchers looked at the behavior of confined concrete under compression and proposed different strength criteria which took account of various parameters such as the uniaxial compressive strength and the level of confinement. One of the earliest equations is the one proposed by Richart *et al.* (1928). The triaxial compression tests performed by the authors showed that an increase of the confinement ratio would increase the peak strength ratio of the specimen an amount 4.1 times the magnitude of the confinement ratio, i.e.,

$$\psi = 1 + 4.1\phi \tag{3}$$

Eq. (3) is a specialization of Mohr-Coulomb failure criterion which may be formulated as below

$$\psi = 1 + k\phi \tag{4}$$

Here, k is model parameter. This formula has been further used in other studies to estimate the strength ratio of actively confined concrete. Balmer (1949) found that k varied between 4.5 and 7 with an average value of 5.6 (higher values correspond to lower confinement pressures). For confinement ratios up to 1, Ansari and Li (1998) reported that the value of k is closer to 2.6 for high-strength concrete (HSC). Candappa *et al.* (2001), studied HSC under confinement ratios of less than 0.2 and recommended the value of 5 for this parameter. Furthermore, in a separate study, $k = 4$ was suggested by Lu and Hsu (2006).

The Leon failure criterion (1935) is also one of the equations used for the prediction of concrete failure surface. It was originally formulated in terms of major and minor principal stresses, σ_1 and σ_3, as below

$$F(\sigma_1, \sigma_3) = \left(\frac{\sigma_1 - \sigma_3}{f_c'}\right)^2 + m\left(\frac{\sigma_1 - \sigma_3}{f_c'}\right) - c = 0 \tag{5}$$

m and c are material constants to be determined. Calibrating the criterion with the experimental data of Hurlbut (1985), Caggiano (2007) suggested the values of 0.857 and 0.143 for the two unknown parameters of m and c, respectively.

Considering c=1, a series of simplified Leon criteria of the form below was suggested.

$$\psi = \phi + \sqrt{1 + m\phi} \tag{6}$$

Caggiano (2007) calibrated this formula, attributed to Hoek and brown (1980), against the experimental data of Hurlburt (1985) and showed that m=6.844. Binici (2005) suggested that m=9.9 for concrete. Girgin *et al.* (2007) employed the results of triaxial tests performed by Xie *et al.* (1995) and Attard and Setunge (1996) to verify the

Table 3 Accuracy of existing and proposed strength criteria

Reference		ψ	Average Absolute Error - Rank													
			Low-confinement ratio								High-confinement ratio					
			$0 \le \phi < 0.25$		$0.25 \le \phi < 0.5$		$0.5 \le \phi < 0.75$		$0.75 \le \phi < 1$		$1 \le \phi < 5$		$5 \le \phi < 10$		$\phi \ge 10$	
Richart *et al.* (1928)		$1 + 4.1\phi$	0.085	1	0.074	3	0.238	12	0.184	15	0.333	15	0.459	14	0.538	12
Caggiano (Leon) (2007)		$\phi + 0.5\sqrt{1.306 + 6.856\phi} + 0.429$	0.144	19	0.289	21	0.313	19	0.313	20	0.420	20	0.453	13	0.494	10
Willam and Warnke (1995)		$\phi + 7.367\sqrt{0.029 + 0.272\phi} - 0.255$	0.125	15	0.105	10	0.250	16	0.155	11	0.200	1	0.169	2	0.269	2
Caggiano (Hoek and Brown 2007)		$\phi + \sqrt{1 + 6.844\phi}$	0.090	3	0.129	16	0.203	4	0.129	5	0.284	12	0.296	8	0.380	8
sHsieh *et al.* (1982)		$\phi + 0.746\sqrt{2.790 + 25.748\phi} - 0.246$	0.122	14	0.099	9	0.241	13	0.150	9	0.201	2	0.173	3	0.274	3
Binici (2005)		$\phi + \sqrt{1 + 9.9\phi}$	0.096	6	0.071	1	0.198	2	0.112	1	0.231	8	0.225	7	0.329	7
Setunge *et al.* (1993)	NSC	$(1 + 13.07\phi)^{0.63}$	0.175	20	0.199	20	0.368	20	0.266	19	0.222	6	0.156	1	0.313	5
	HSC with SF	$(1 + 18.67\phi)^{0.45}$	0.128	16	0.075	4	0.194	1	0.121	3	0.370	16	0.534	17	0.688	16
	HSC without SF	$(1 + 14.67\phi)^{0.45}$	0.093	5	0.115	13	0.207	5	0.178	13	0.419	19	0.581	18	0.720	17
Xie *et al.* (1995)		$\sqrt{1 + (21.2 - 0.05f_c')\phi}$	0.180	21	0.135	17	0.247	14	0.125	4	0.268	10	0.385	10	0.576	14
Attard and Setunge (1996)	HSC with SF	$\left(1 + f_l/0.558\sqrt{f_c'}\right)^{1.25(1+0.062\phi)(f_c')^{-0.21}}$	0.100	9	0.080	7	0.217	7	0.131	6	0.208	4	0.716	19	14.646	20
	HSC without SF	$\left(1 + f_l/0.288f_c'^{0.67}\right)^{1.25(1+0.062\phi)(f_c')^{-0.21}}$	0.114	12	0.087	8	0.268	17	0.144	8	0.276	11	0.771	21	16.639	21
Ansari and Li (1998)		$1 + 2.45\phi^{0.703}$	0.097	7	0.138	18	0.218	9	0.184	15	0.371	17	0.460	15	0.571	13
Li and Ansari (2000)		$1 + 2.43\phi^{0.6376}$	0.119	13	0.120	14	0.211	6	0.183	14	0.397	18	0.518	16	0.639	15
Candappa *et al.* (2001)		$1 + 5\phi$	0.097	7	0.126	15	0.404	21	0.386	21	0.576	21	0.768	20	0.870	19
Imran and Pantazopoulou (1996)		$\phi + \sqrt{1.043 + 10.571\phi} - 0.021$	0.102	10	0.072	2	0.202	3	0.118	2	0.223	7	0.213	6	0.320	6
Tan (2005)		$-2\phi + 10.338\sqrt{1 + 1.368\phi} - 9.338$	0.090	3	0.076	5	0.217	7	0.132	7	0.255	9	0.451	12	0.788	18
Lu and Hsu (2006)		$1 + 4\phi$	0.086	2	0.076	5	0.227	10	0.168	12	0.307	13	0.425	11	0.501	11
Girgin *et al.* (2007)		$1 + 4.08\phi^{0.83}$	0.133	17	0.111	12	0.286	18	0.202	18	0.208	4	0.164	4	0.084	1
		$\phi + \sqrt{1 + 13\phi}$	0.136	18	0.110	11	0.248	15	0.152	10	0.204	3	0.181	5	0.286	4
Singh *et al.* (2011)		$\phi + \sqrt{1 + 5.16\phi}$	0.106	11	0.180	19	0.232	11	0.185	17	0.323	14	0.343	9	0.413	9
Proposed Model		$\phi + \sqrt{1 + 9.3\phi\exp(0.089\phi)}$	**0.091**		**0.074**		**0.198**		**0.113**		**0.204**		**0.157**		**0.069**	

applicability of Eq. (6) to HSC. As a result, they found the best value of m to be 13. Also, the value of 5.16 was suggested for m by Singh *et al.* (2011).

Willam and Warnke (1995) introduced a five-parameter failure surface whose compressive meridian was a parabolic function of the form below

$$\sigma_m = b_0 + b_1\rho_c + b_2{\rho_c}^2 \tag{7}$$

Here, σ_m and ρ_c are the mean stress and the deviatoric stress invariant in the Haigh-Westergaard coordinate system, respectively. b_i (i=0,1,2) are material constants. They calibrated the model for NSC and showed that b_0=0.1025, b_1=−0.4507, and b_2=−0.1028. Hence, their criterion can be written as

$$\psi = \phi + 7.3674\sqrt{0.0290 + 0.2715\phi} - 0.2554 \tag{8}$$

Tan (2005) performed three sets of experiments on NSC and HSC, then employed Willam-Warnke's criterion, and finally proposed their relation in the following form

$$\psi = -2\phi + 10.338\sqrt{1 + 1.368\phi} - 9.338 \tag{9}$$

In a separate study on NSC, Hsieh *et al.* (1982) proposed the following four-parameter failure function

$$aJ_2 + b\sqrt{J_2} + c\sigma_1 + dI_1 - 1 = 0 \tag{10}$$

where, σ_1, I_1, and J_2 are the maximum principal stress, the first invariant of the stress tensor, and the second invariant of the deviatoric stress tensor, respectively. Calibration of the model showed that a=2.0108, b=0.9714, c=9.1412, and d=0.2312.

Using the mathematical form of Eq. (10) and the experimental background of 130 triaxial tests performed on cylindrical specimens, Imran and Pantazopoulou (1996) proposed the equation below for the strength of confined concrete

$$\psi = \phi + \sqrt{1.043 + 10.571\phi} - 0.021 \tag{11}$$

Setunge *et al.* (1993) suggested the following relations for NSC and HSC.

$$\psi = (1 + 13.07\phi)^{0.63} \quad \text{for} \quad \text{NSC} \tag{12}$$

$$\psi = (1 + 18.67\phi)^{0.45} \quad \text{for} \quad \text{HSC with silica fume} \tag{13}$$

$$\psi = (1 + 14.67\phi)^{0.45} \quad \text{for} \quad \text{HSC without silica fume} \tag{14}$$

In 1996, the following criterion for the strength of confined concrete subjected to low confining pressure was proposed by Attard and Setunge (1996) and shown to be applicable to the wide range of concrete strengths between 20 and 130 MPa.

$$\psi = \left(1 + \frac{f_l}{f_t}\right)^k, k = 1.25(1 + 0.062\phi)(f_c')^{-0.21} \quad (15)$$

f_t is the tensile strength of concrete. They also suggested that depending on whether silica fume is used in concrete mixture or not, one of the following equations should be employed for f_t.

$$f_t = 0.288(f_c')^{0.67} \quad \text{without silica fume} \quad (16)$$

$$f_t = 0.558\sqrt{f_c'} \quad \text{with silica fume} \quad (17)$$

Ansari and Li (1998) and Li and Ansari (2000) also proposed the following two equations as the best fits of HSC data using nonlinear regression analysis

$$\psi = 1 + 2.45\phi^{0.703} \quad (18)$$

$$\psi = 1 + 2.4305\phi^{0.6376} \quad (19)$$

Now, let's focus on the accuracy of these existing strength criteria. For this reason, the average absolute error (AAE) defined below is used.

$$\mathrm{AAE} = \frac{1}{N}\sum_{i=1}^{N}\left|\frac{\psi_i^{\mathrm{M}} - \psi_i^{\mathrm{E}}}{\psi_i^{\mathrm{E}}}\right| \quad (20)$$

Superscripts M and E stand for the model predicted and experimentally obtained values, respectively. N is the total number of datasets. Using Eq. (20), the errors of abovementioned criteria and their ranks are calculated and tabulated in Table 3. It has to be noted that, to get more insight from our comparison, the AAE has been reported at seven separate ranges of confinement ratios. Moreover, in this table, the three best and worst criteria of each confinement interval are highlighted in blue and red, respectively. Alongside, Fig. 3 compares the analytical curves with the experimental data.

The data of Table 3 show that the existing criteria yield comparatively different predictions. Although some equations do make reasonable predictions within specific ranges of confinement ratios, they lose their accuracy in other ranges. In particular, using existing criteria except one proposed by Girgin *et al.* (2007) for HSC, strength under high confinement pressures are poorly predicted (see Fig. 3(b)).

According to Table 3, among the existing models, the criteria proposed by Imran and Pantazopoulou (1996) and Binici (2005) showed promising results at low-confinement ratios. As already discussed, the Binici criterion belongs to the family of Leon criteria with the simple mathematical form of Eq. (6). Thus, assuming that m in Eq. (6) is an independent variable, one can rewrite this equation as below

$$m = \frac{(\psi - \phi)^2 - 1}{\phi} \quad (21)$$

The values of this parameter have been calculated for all the experimental ψ-ϕ pairs of the database and displayed in Fig. 4. As can be seen, for low-confinement ratios, the computed values of m are dispersed around 10, however, as ϕ increases, higher values are obtained. As a result, a criterion in the form of Eq. (6) with a constant m would be an inefficient solution for the accurate estimation of experimental results within the whole range of confinement ratios. Motivated by this observation, the following simple yet flexible two-parameter function of ϕ is suggested for m.

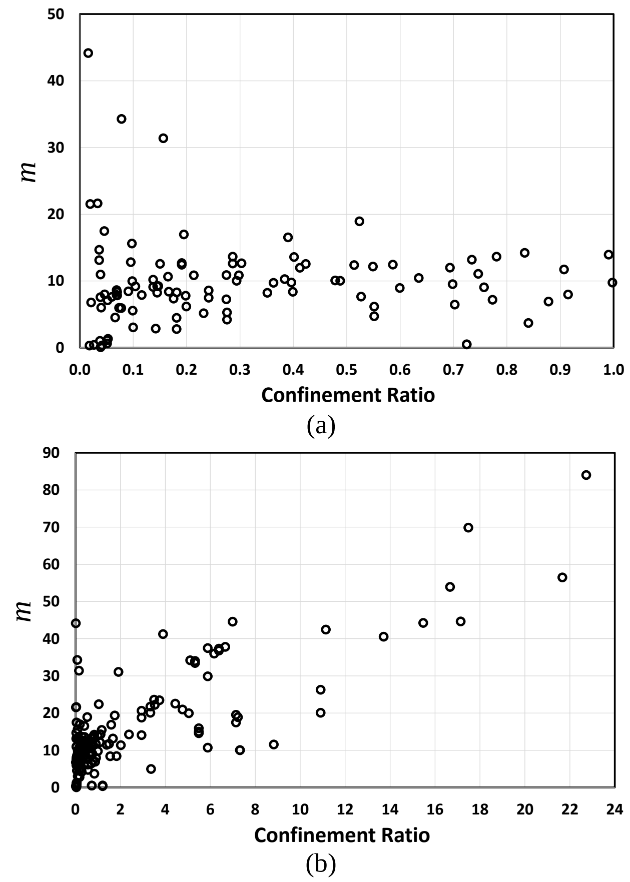

Fig. 4 Parameter m calculated from the test results. (a) Low-confinement ratios and (b) all confinement ratios

$$m = M\exp(N\phi) \quad (22)$$

The two constants of Eq. (22), M and N, adjusted in accord with the database of experimental results are 9.3 and 0.089, respectively. Back-substitution of these calibrated values in Eq. (6), the final form of our unified strength criterion for NSC could be presented as below

$$\psi = \phi + \sqrt{1 + 9.3\phi\exp(0.089\phi)} \quad (23)$$

The prediction of this criterion is also provided in Fig. 3 and the corresponding errors are presented in the last row of Table 3. These results confirm that, in contrary to the existing strength criteria, the suggested unified model provides sufficient accuracy for the whole range of ϕ. It has to be noted that, as physically expected, the form of proposed model for ϕ is similar to that of a hydrostatically loaded concrete, the fact that was ignored in previous models.

3.2 Peak strain criterion

A representative peak strain criterion is one of the key

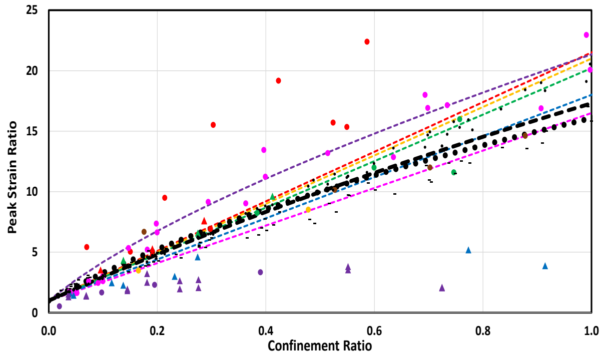

(a)

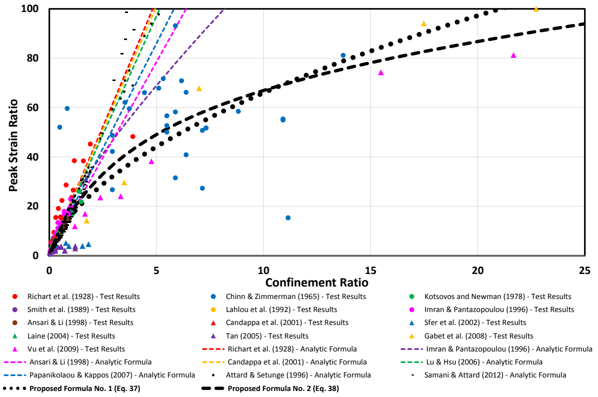

(b)

Fig. 5 Predictions of the models for the peak strain ratio. (a) Low-confinement ratios ($\phi \leq 1$) and (b) all confinement ratios

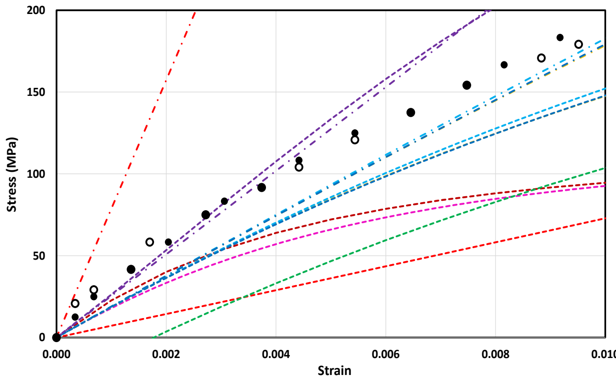

(a)

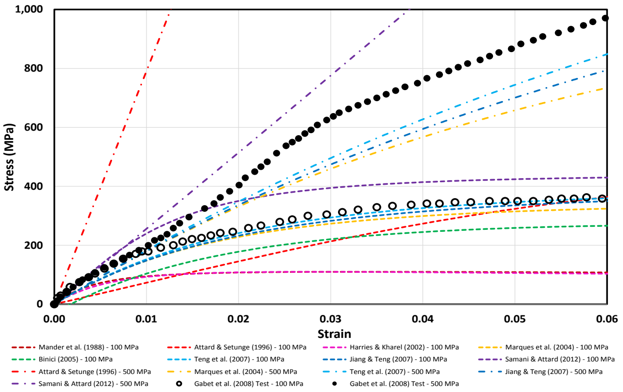

(b)

Fig. 6 Predictions of existing models for the stress-strain curves of two actively confined samples tested in Gabet *et al.* (2006) (f_c'=28.6, f_{l1}=100, and f_{l2}=500MPa). Strain ranges of (a) (0,0.01) and (b) (0,0.06)

elements in the modeling of stress-strain curves of actively confined concrete. One of the mathematical forms frequently used for the peak strain ratio is the following linear function of the confinement ratio

$$\chi = 1 + \alpha\phi \tag{24}$$

Here, α is model parameter to be estimated. Depending on the experimental database used in the calibration of this equation, several values have already been suggested for α. Some examples of this kind are listed below.

$$\chi = 1 + 20.5\phi,\ \text{Richart } et\ al.\ (1928) \tag{25}$$

$$\chi = 1 + 15.5\phi,\ \text{Ansari and Li (1996)} \tag{26}$$

$$\chi = 1 + 20\phi,\ \text{Candappa } et\ al.\ (2001) \tag{27}$$

$$\chi = 1 + 19.2\phi,\ \text{Lu and Hsu (2006)} \tag{28}$$

$$\chi = 1 + 17\phi,\ \text{Papanikolaou and Kappos (2007)} \tag{29}$$

Alongside, the following nonlinear formulas are available in the literature.

$$\chi = 1 + (17 - 0.06f_c')\phi,\ \text{Attard and Setunge (1996)} \tag{30}$$

$$\chi = 6\left(\phi + \sqrt{1.043 + 10.571\phi} - 0.851\right),\ \text{Imran and Pantazopoulou (1996)} \tag{31}$$

$$\chi = e^{\left[(2.9224 - 0.00367f_c')\phi^{(0.3124+0.002\phi)}\right]},\ \text{Samani and Attard (2012)} \tag{32}$$

As can be seen, some of these equations depend not only on the confinement ratio but also consider the effect of uniaxial compressive strength as an extra independent variable.

Now, let's compare the predictions of these formulas with the experimentally measured values gathered from different studies. It should be noted that the scatter observed in the values of measured peak strains is not surprising as, in contrary to failure strength, accurate measuring/recording of peak strains in actual confined concrete tests is a tedious task. Fig. 5(a)-5(b) present the comparisons for low-confinement ratios and whole range of ϕ values, respectively.

Fig. 5(a) confirms that, when $\phi \leq 1$, all the mentioned peak strain formulas make relatively good estimations and move within the experimental values, but, as revealed in Fig. 5(b), they fail to predict the trend of experimental results at higher confinement ratios. This finding has the potential to motivate new systematic experimental studies at higher ϕ values, however, for the time being, we have used the existing test results and tried different mathematical forms from which the following equations are found flexible enough for the prediction of measured values in the whole range of confinement ratios.

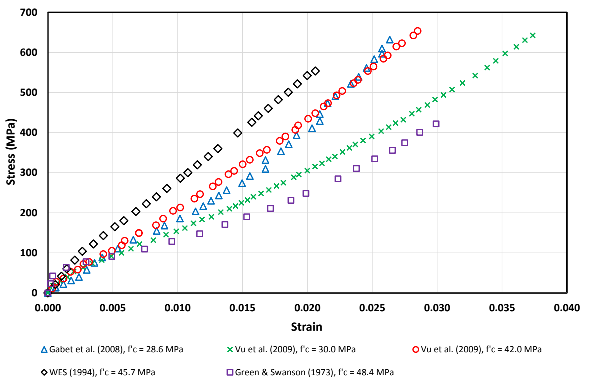

Fig. 7 Examples of hydrostatic stress-strain curves for NSC

$$\chi = a\left(\phi + \sqrt{b + c\phi} + \frac{1}{a} - \sqrt{b}\right) \tag{33}$$

$$\chi = 1 + a\left\{1 - \exp\left[-b\phi\left(\frac{c\phi + d}{\phi + d}\right)\right]\right\} \tag{34}$$

a, b, c, and d are model parameters. Calibrating these two equations against the experimental results, the following forms are finally suggested.

$$\chi = 0.063\left(\phi + 100\sqrt{3.035 + 13.99\phi} - 158.33\right) \tag{35}$$

$$\chi = 1 + 200\left\{1 - \exp\left[-\frac{0.01\phi^2 + 0.5\phi}{\phi + 5}\right]\right\} \tag{36}$$

The efficiency of above formulas are shown in Fig. 5.

3.3 Backbone hydrostatic curve

To the best of our knowledge, the backbone hydrostatic curve is a new element brought to the modelling of actively confined concrete in this study. This new element ensures that a stress-strain curve is physically representative in its first phase of loading (see Fig. 1).

To shed more light on the importance of this element, let's compare the predictions of existing models with the test results of Gabet *et al.* (2006) on two highly confined samples as shown in Fig. 6 (f_c'=28.6, f_{l1}=100, and f_{l2}=500 MPa). This figure reveals that, most of existing criteria are impotent to trace the experimental curves especially for the confining stress of 500 MPa. It should be noted that some of the models yield improper values (negative or complex numbers) and are not shown in Fig. 6.

Experimentally measured hydrostatic stress-strain curves of concrete are quite limited in the literature (see e.g., Green and Swanson 1973, Gabet *et al.* 2006, and Vu *et al.* 2009). Some of these curves for NSC are shown in Fig. 7. As observed, one can find concrete samples with comparable uniaxial strengths but completely different hydrostatic responses (see also Malecot *et al.* 2009). This fact can be attributed to the differences in mesostructures and specifically the void content of samples which controls the slope of pore collapse phase and also the densification strain (Fig. 1). Hence, for the proposed model to be accurate enough in both low and high-confinement ratios, the hydrostatic stress-strain curve should be separately provided. However, in light of future research, it may be possible to propose representative models for the hydrostatic curve of concrete. Such models should undoubtedly depend on more parameters rather than just unconfined compressive strength.

3.4 Transient hardening curve

The transient hardening curve links the point of departure from the hydrostatic curve to the peak point of the actively confined stress-strain curve. Giving the uniaxial compressive strength of concrete and the confining stress, one can easily calculate the coordinates of both departure and peak points using the hydrostatic curve and the formulas suggested in Sections 3.1 and 3.2 for the peak stress and peak strain, respectively. Moreover, we know that the slope of transient curve vanishes at the peak point. Accordingly, in this section first we introduce our assumptions for the slope of actively confined stress-strain curve at the point of departure, and next, a conforming mathematical equation will be suggested for the transient curve.

The first issue regarding the initial slope of the transient curve is when an actively confined concrete leaves the elastic region and experiences permanent deformations. The assumption we made here is that, regardless of the level of confinement, the strain corresponding to the end of elastic region is constant and equal to ε_c^e. This includes the two extreme cases of uniaxial (ϕ=0) and hydrostatic loading conditions ($\phi\to\infty$). This assumption has been graphically illustrated in Fig. 8. Based on this hypothesis, for confining stresses less than f_l^e=$E_c\,\varepsilon_c^e$/(1−2ν), the initial slope of transient hardening curve would be equal to the Young's modulus, E_c, which is ξ=1−2ν times that of the elastic part of hydrostatic curve. It is further assumed that, for confining stresses higher than f_l^e, the initial slope of transient curve is ξ times the tangent slope of hydrostatic curve at the point of departure (see Fig. 8).

The next step is to introduce an appropriate equation for the transient part. Before proceeding further, it should be noted that, for confining stresses less then f_l^e, the transient hardening curve is made up of a linear elastic segment in its initial part with the slope of E_c (see Fig. 8) and a nonlinear curve for the strain range of (ε_c^e, ε'_{cc}). Hence, in what follows, we will look for a representing mathematical formula for the nonlinear part of transient curves.

Let's first examine the following equations previously used in Binici (2005) and Samani and Attard (2012) for the ascending part of actively confined stress-strain curves.

$$\sigma = \sigma_n + \frac{\bar{E}\bar{x}}{\bar{E}-1+\bar{x}^{\bar{E}}}\left(f'_{cc} - \sigma_n\right),\quad \bar{E} = \frac{E_n}{E_n - \dfrac{f'_{cc}-\sigma_n}{\varepsilon'_{cc}-\varepsilon_n}},\quad \bar{x} = \left(\frac{\varepsilon - \varepsilon_n}{\varepsilon'_{cc} - \varepsilon_n}\right) \tag{37}$$

$$\sigma = \sigma_n + \frac{A\bar{x}+B\bar{x}^2}{1+(A-2)\bar{x}+(B+1)\bar{x}^2}\left(f'_{cc} - \sigma_n\right),\quad A = \frac{\varepsilon'_{cc}-\varepsilon_n}{f'_{cc}-\sigma_n}E_n,\quad B = \frac{(A-1)^2}{0.55} - 1 \tag{38}$$

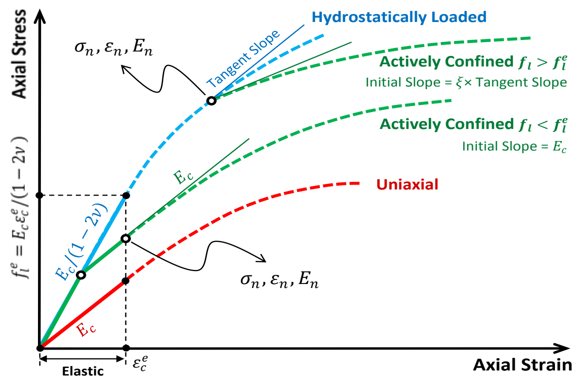

Fig. 8 Initial slope of transient hardening curves in the proposed model

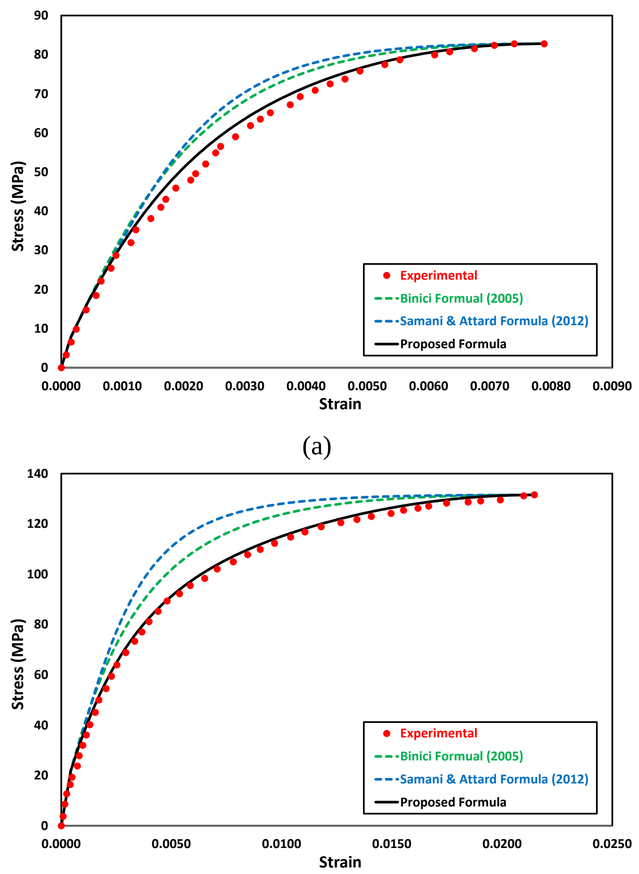

(a)

(b)

Fig. 9 Comparison of predicted ascending stress-strain curves with the experimental results of Lahlou *et al.* (1992) ($f_c' = 46$ MPa). (a) $f_l = 7.6$ MPa and (b) $f_l = 22$ MPa

σ_n, ε_n, and E_n are the initial stress, strain, and slope of the nonlinear part of transient curve, respectively. Since the efficiency of formulas would be examined in this section, the peak strains and stresses are directly taken from the corresponding test results. The value of ε_c^e is reasonably assumed to be $0.3f_c'/E_c$ (Chen and Han 1988). Moreover, uniaxial elastic moduli, E_c, and uniaxial peak strains, ε_c', are calculated form the following equations borrowed from ACI 318 (2011) and Binici (2005), respectively.

$$E_c = 4700\sqrt{f_c'} \tag{39}$$

$$\varepsilon_c' = 10^{-6}\left(-0.067f_c'^{2} + 29.9f_c' + 1053\right) \tag{40}$$

Figs. 9-10 compare predicted curves with the experimental results of Lahlou *et al.* (1992) and Smith *et al.* (1989), respectively. They show that Eqs. (37)-(38) perform well at low-confinement ratios, but, lose their accuracy at higher confinements. Unsurprisingly, this weak point also exists in the predictions of actively confined models proposed in Binici (2005) and Samani and Attard (2012) (see e.g., Figs. 4 and 7 of Binici 2005 and Figs. 30 and 34 of Samani and Attard 2012). Accordingly, the mathematical form of Eq. (37) has been systematically upgraded to the form below which can adequately simulate transient hardening curves at all confinement ratios (see Figs. 9-10).

$$\sigma = \sigma_n + \left\{1 - 0.15[1-\exp(-10\phi)]\cos^2\left(\frac{\pi}{2}\bar{x}\right)\right\}\frac{\bar{E}\bar{x}}{\bar{E}-1+\bar{x}^{\bar{E}}}\left(f_{cc}'-\sigma_n\right) \tag{41}$$

3.5 Post-peak softening curve

The post-peak softening curve of confined concrete determines the pace at which stress decreases beyond the peak point and reaches its final residual strength, f_{res}. Many formulas have been already proposed for the post-peak region of actively confined concrete from which the one suggested by Samani and Attard (2012) may be considered one of the most recent and physically-based models (see a complete discussion regarding this issue in Section 5 of Samani and Attard 2012). The model considers the effect of confining stress on concrete post-peak compression fracture energy and also takes account of sample size. Samani and Attard (2012) formulated their model for the normal-weight concrete in the following mathematical form

$$\sigma = f_{res} + (f_{cc}' - f_{res})\left[\frac{f_{ic}}{f_c'}\right]^{\left(\frac{\varepsilon-\varepsilon_{cc}'}{\varepsilon_i-\varepsilon_{cc}'}\right)^2}, \varepsilon \geq \varepsilon_{cc}' \tag{42}$$

where

$$f_{ic} = (1.41 - 0.17\ln f_c')f_c', \qquad f_c' \geq 20 \text{ MPa}, \tag{43}$$

$$\frac{\varepsilon_i}{\varepsilon_{cc}'} = \left(1.26 + \frac{2.89}{\sqrt{f_c'}}\right)\frac{f_{res}}{f_{cc}'} + \left(1 - \frac{f_{res}}{f_{cc}'}\right)\frac{\varepsilon_{ic}}{\varepsilon_c'},$$

$$\varepsilon_{ic} = \begin{cases}(2.76 - 0.35\ln f_c')\dfrac{f_c'}{E_c}\dfrac{4.26}{\sqrt[4]{f_c'}} & \text{Crushed Aggregates}\\[2ex] (2.76 - 0.35\ln f_c')\dfrac{f_c'}{E_c}\dfrac{3.78}{\sqrt[4]{f_c'}} & \text{Gravel Aggregates}\end{cases} \tag{44}$$

$$f_{res} = \left\{1 - \frac{1}{[795.7 - 3.291f_c']\phi^{(5.79\phi^{0.694}+1.301)} + 1}\right\}f_{cc}' \tag{45}$$

f_{ic} and ε_{ic} are the stress and strain of inflexion point of uniaxial softening curve, respectively, and ε_i is the strain of inflexion point of confined condition.

Next, considering the empirical results of Vonk (1992) and the Compression Damage Zone (CDZ) model proposed

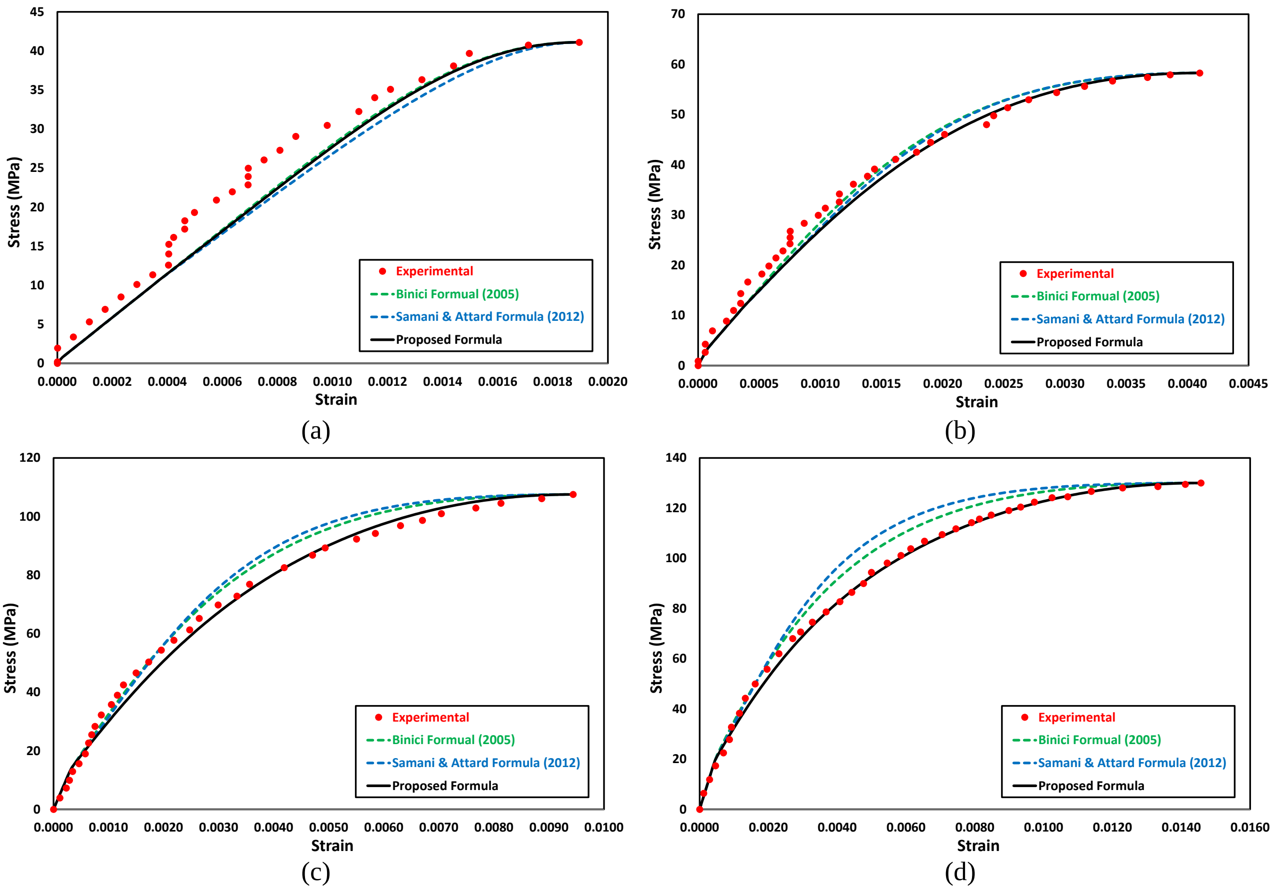

Fig. 10 Comparison of predicted ascending stress-strain curves with the experimental results of Smith *et al.* (1989) ($f_c' = 34.5$ MPa). (a) $f_l = 0.69$ MPa, (b) $f_l = 3.45$ MPa, (c) $f_l = 13.45$ MPa, and (d) $f_l = 20.7$ MPa

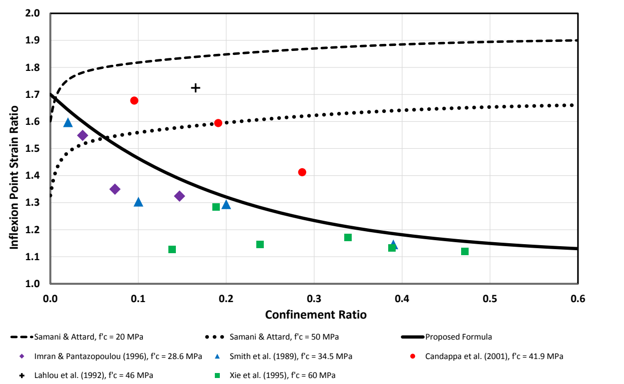

Fig. 11 Comparison of NSC experimental results with the predictions of formula proposed by Samani and Attard (2012) and Eq. (48) proposed in this study for inflexion point strain ratio

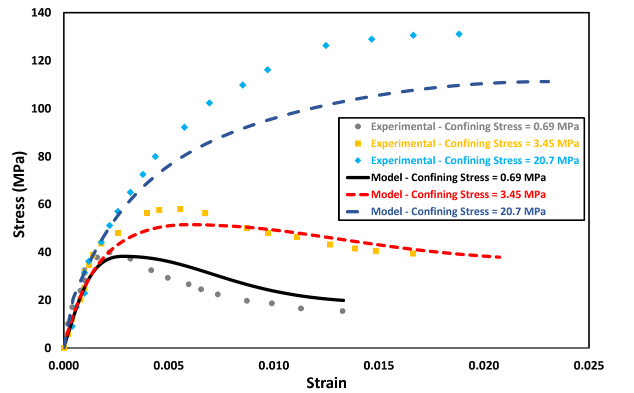

Fig. 12 Predictions of proposed model for the stress-strain curves of Smith *et al.* (1989) ($f_c' = 34.5$ MPa)

by Markeset and Hillerborg (1995) which indicate that for the uniaxial case, the compressive fracture energy per unit area for specimens of the same aspect ratio greater than or equal to 2 but of different heights, is not the same, Samani and Attard (2012) proposed the following equations to adjust total strain, ε_h, for a specimen of height h.

$$\varepsilon_h = \begin{cases} \varepsilon_{cc}' + (\varepsilon - \varepsilon_{cc}')\frac{h_r}{h} + \frac{(\sigma - f_{cc}')}{E_c}\left[1 - \frac{h_r}{h}\right] + \varepsilon_d\left(\frac{h_d}{h} - \frac{h_r}{h}\right), & h > h_d \\ \varepsilon_{cc}' + (\varepsilon - \varepsilon_{cc}')\frac{h_r}{h} + \frac{(\sigma - f_{cc}')}{E_c}\left[1 - \frac{h_r}{h}\right] + \varepsilon_d\left(1 - \frac{h_r}{h}\right), & h \le h_d \end{cases} \quad (46)$$

$$\varepsilon_d = \frac{6}{5}\frac{G_{ft}}{f_{cc}'}\left(\frac{f_{cc}' - \sigma}{f_{cc}' - f_{res}}\right)^{0.8}, \qquad G_{ft} = 0.00097 f_c' + 0.0418 \quad (47)$$

h_d is the damage zone height taken as two times the width or diameter of the specimen. h_r is a characteristic length of 200 mm representing the most typical specimen height used in the compressive testing. It needs to note that, when such a model is applied for structural analysis of beams and columns, h and h_d should be taken as the length and width of the compressed region, respectively.

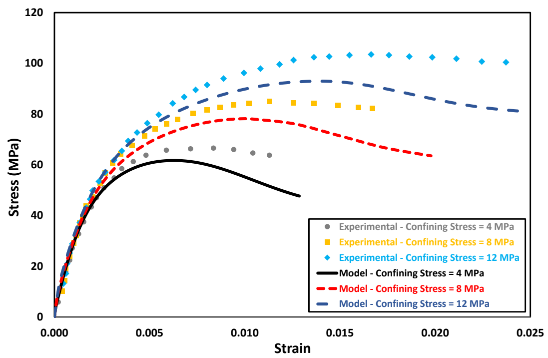

Fig. 13 Predictions of proposed model for the stress-strain curves of Candappa *et al.* (2001) (f_c'=41.9 MPa)

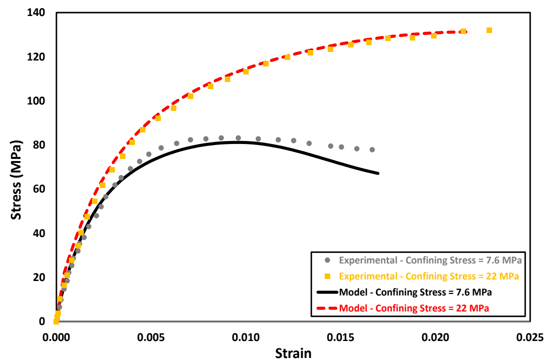

Fig. 14 Predictions of proposed model for the stress-strain curves of Lahlou *et al.* (1992) (f_c'=46 MPa)

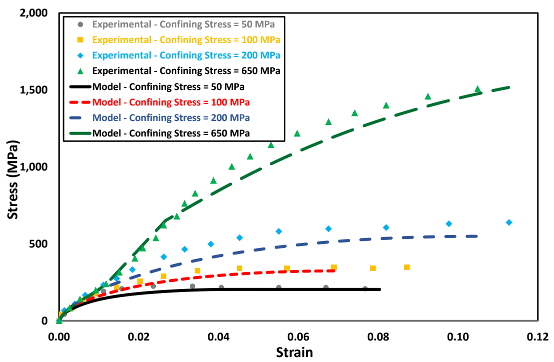

Fig. 15 Predictions of proposed model for the stress-strain curves of Vu *et al.* (2009) (f_c'=42 MPa)

Samani and Attard (2012) suggested Eq. (44) for the dependency of ε_i on confinement ratio and uniaxial compressive strength, however, they mainly used the results of HSC in their development. Hence, in this part, more experimental data would be incorporated to assess the accuracy of Eq. (44) for NSC.

Fig. 11 presents the inflexion point strains of tested NSC samples and compares them with the predictions of Eq. (44). As can be seen, the calculated values of $\varepsilon_i/\varepsilon'_{cc}$ (inflexion point strain ratio) vary within the interval of 1.1 to 1.7 without any clear dependency on f_c' while Eq. (44) predicts larger values for weaker concrete samples. On the other hand, this figure shows that the value of $\varepsilon_i/\varepsilon'_{cc}$ decreases as confinement ratio grows. Hence, in this study, the following function of ϕ has been fitted to the data and suggested for the inflexion point strain ratio of NSC.

$$\frac{\varepsilon_i}{\varepsilon'_{cc}} = 1.1 + 0.6\exp(-5\phi) \tag{48}$$

4. Model verification

Although different elements of the proposed model are separately verified in previous parts, Figs. 12-15 compare the predictions of model with the experimental stress-strain curves of Smith *et al.* (1989), Candappa *et al.* (2001), Lahlou *et al.* (1992), and Vu *et al.* (2009), respectively. These figures confirm that the predictions of proposed model are satisfactorily conforming to the test results for both low and high-confinement ratios.

5. Conclusions

The current study proposes a new stress-strain model for actively confined normal-strength concrete in the axial direction whose main elements are inspired by the loading path traveled in a typical fluid confined test. The first part of the paper examines the initial elastic response of existing analysis-oriented models. It is clarified that all of the models mistakenly yield values equal to the Young's modulus. Next, using a database containing more than 160 experimental datasets from the literature with a broad range of confinement ratios, new formulas are introduced for the peak stress and peak strain of normal strength confined concrete. A backbone hydrostatic curve is incorporated to make it possible to correctly simulate the initial loading phase of the tests. A transient hardening curve linking the point of departure from the hydrostatic curve to the peak/failure point of confined concrete is also introduced in a separate part. The post-peak equations of the model are the last components formulated in accord to the existing experimental evidences. Finally, in a separate verification section, comparisons are made between the predictions of proposed model and different test results from the literature.

References

ACI 318-11 (2011), *Building Code Requirements for Structural Concrete*, American Concrete Institute, Farmington Hills, Michigan, U.S.A.

Albanesi, T., Nuti, C. and Vanzi, I. (2007), "Closed form constitutive relationship for concrete filled FRP tubes under compression", *Constr. Build. Mater.*, **21**(2), 409-427.

Ansari, F. and Li, Q. (1998), "High-strength concrete subjected to triaxial compression", *ACI Mater. J.*, **95**(6), 747-755.

Attard, M.M. and Setunge, S. (1996), "Stress-strain relationship of confined and unconfined concrete", *ACI Mater. J.*, **93**(5), 432-442.

Balmer, G.G. (1949), *Shearing Strength of Concrete under High Triaxial Stress-Computation of Mohr's Envelope as a Curve*, Technical Report No. SP-23, Structure Research Laboratory, Denver, Colorado, U.S.A.

Binici, B. (2005), "An analytical model for stress-strain behavior of confined concrete", *Engineering Structures*, **27**(7), 1040-1051.

Caggiano, A. (2007), "Application of some classic constitutive theories to the numerical simulation of the behavior of plain concrete", M.S. Dissertation, University of Salerno, Salerno, Italy.

Candappa, D.C., Sanjayan, J.G. and Setunge, S. (2001), "Complete triaxial stress-strain curves of high-strength concrete", *ASCE J. Mater. Civil Eng.*, **13**(3), 209-215.

Chen, W.F. and Han, D.J. (1988), *Plasticity for Structural Engineers*, Springer-Verlag, New York, U.S.A.

Chinn, J. and Zimmerman R.M. (1965), "Behavior of plain concrete under various high triaxial compression loading conditions", Technical Report No. WL-TR-64-163, Air Force Weapons Laboratory, New Mexico.

Ding, F., Tan, L., Liu, X. and Wang, L. (2017), "Behavior of circular thin-walled steel tube confined concrete stub columns", *Steel Compos. Struct.*, **23**(2), 229-238.

Dupray, F., Malécot, Y., Daudeville, L. and Buzaud, E. (2009), "A mesoscopic model for the behaviour of concrete under high confinement", *J. Numer. Analy. Meth. Geomech.*, **33**(11), 1407-1423.

Fam, A.Z. and Rizkalla, S.H. (2001) "Confinement model for axially loaded concrete confined by circular fiber-reinforced polymer tubes", *ACI Struct. J.*, **9**(4), 451-461.

Gabet, T., Malécot, Y. and Daudeville, L. (2008), "Triaxial behavior of concrete under high stresses: Influence of the loading path on compaction and limit states", *Cement Concrete Res.*, **38**(3), 403-412.

Gabet, T., Vu, X.H., Malécot, Y. and Daudeville, L. (2006), "A new experimental technique for the analysis of concrete under high triaxial loading", *J. De Phys. IV*, **134**, 635-640.

Ghorbi, E., Soltani, M. and Maekawa, K. (2013), "Development of a compressive constitutive model for FRP-confined concrete elements", *Compos. Part B: Eng.*, **45**(1), 504-517.

Girgin, Z.C., Anoglu, N. and Anoglu, E. (2007), "Evaluation of strength criteria for very-high-strength concretes under triaxial compression" *ACI Struct. J.*, **104**(3), 277-283.

Green, S.I. and Swanson, S.R. (1973), *Static Constitutive Relations for Concrete*, Report No. AFWL-TR-72-2, Air Force Weapons Lab, Kirtland Air Force Base, Albuquerque, New Mexico.

Hansen, T.C. (1995), *Triaxial Tests with Concrete and Cement Paste*, Report No. 319, Technical University of Denmark, Denmark.

Harries, K.A. and Kharel, G. (2002), "Behavior and modeling of concrete subject to variable confining pressure", *ACI Mater. J.*, **99**(2), 180-189.

Hoek, E. and Brown, E.T. (1980), "Empirical strength criterion for rock masses", *ASCE J. Geotech. Eng.*, **106**(9), 1013-1035.

Hsieh, S.S., Ting, E.C. and Chen, W.F. (1982), "A plasticity-fracture model for concrete", *J. Sol. Struct.*, **18**(3), 181-197.

Hurlbut, B. (1985), "Experimental and computational investigation of strain-softening in concrete", M.S. Dissertation, University of Colorado, U.S.A.

Imran, I. and Pantazopoulou, S.J. (1996), "Experimental study of plain concrete under triaxial stress", *ACI Mater. J.*, **93**(6), 589-60.

Jiang, T. and Teng, J.G. (2007), "Analysis-oriented stress-strain models for FRP-confined concrete", *Eng. Struct.*, **29**(11), 2968-2986.

Kotsovos, M.D. and Newman, J.B. (1978), "Generalized stress-strain relations for concrete", *ASCE J. Eng. Mech.*, **104**(4), 845-856.

Lahlou, K., Aïtcin, P.C. and Chaallal, O. (1992), "Behaviour of high-strength concrete under confined stresses", *Cement Concrete Compos.*, **14**(3), 185-193.

Laine, D.P. (2004), "Effect of axial preloads on confined concrete", M.S. Dissertation, University of Toronto, Canada.

Leon, A. (1935), "Uber die scherfestigkeit des betons", *Beton Eisen*, **34**(8).

Li, Q. and Ansari, F. (2000), "High-strength concrete in triaxial compression by different sizes of specimens", *ACI Mater. J.*, **97**(6), 684-689.

Lu, X. and Hsu, C.T.T. (2006), "Behavior of high-strength concrete with and without steel fiber reinforcement in triaxial compression", *Cement Concrete Res.*, **36**(9), 1679-1685.

Malecot, Y., Vu, X.H. and Daudeville, L. (2009), "Unconfined compressive strength is a poor indicator of the high-pressure mechanical response of concrete", *DYMAT*, **2**, 1325-1331.

Mander, J.B., Priestley, M.J.N. and Park, R. (1988), "Theoretical stress-strain model for confined concrete", *ASCE J. Struct. Eng.*, **114**(8), 1804-1826.

Markeset, G. and Hillerborg, A. (1995), "Softening of concrete in compression-localization and size effects", *Cement Concrete Res.*, **25**(4), 702-708.

Marques, S.P.C., Marques, D.C.S.C., Da Silva, J.L. and Cavalcante, M.A.A. (2004), "Model for analysis of short columns of concrete confined by fiber-reinforced polymer", *ASCE J. Compos. Constr.*, **8**(4), 332-340.

Montuori, R., Piluso, V. and Tisi, A. (2012), "Comparative analysis and critical issues of the main constitutive laws for concrete elements confined with FRP", *Compos. Part B: Eng.*, **43**(8), 3219-3230.

Montuori, R., Piluso, V. and Tisi, A. (2013), "Ultimate behaviour of FRP wrapped sections under axial force and bending: Influence of stress-strain confinement model", *Compos. Part B: Eng.*, **54**(1), 85-96.

Ozbakkaloglu, T., Lim, J.C. and Vincent, T. (2013), "FRP-confined concrete in circular sections: Review and assessment of stress-strain models", *Eng. Struct.*, **49**, 1068-1088.

Papanikolaou, V.K. and Kappos, A.J. (2007), "Confinement-sensitive plasticity constitutive model for concrete in triaxial compression", *J. Sol. Struct.*, **44**(21), 7021-7048.

Richart, F.E., Brandtzaeg, A. and Brown, R.L. (1928), *A Study of the Failure of Concrete under Combined Compressive Stresses*, Engineering Experimental Station Bulletin No.185, University of Illinois.

Sadeghi, K. and Nouban, F. (2017), "Behavior modeling and damage quantification of confined concrete under cyclic loading", *Struct. Eng. Mech.*, **61**(5), 625-635.

Samani, A.K. and Attard, M.M. (2012), "Stress-strain model for uniaxial and confined concrete under compression", *Eng. Struct.*, **41**, 335-349.

Samdani, S. and Sheikh, S.A. (2005), "Analytical study of FRP confined concrete columns", *Proceedings of the 4th Conference on Our World in Concrete and Structures*, Seoul, South Korea.

Setunge, S., Attard, M.M. and Darvall, P.P. (1993), "Ultimate strength of confined very high-strength concretes", *ACI Struct. J.*, **90**(6), 632-641.

Sfer, D., Carol, I. and Etse, G. (2002), "Study of the behavior of concrete under triaxial compression" *ASCE J. Eng. Mech.*, **128**(2), 156-163.

Shin, M. and Andrawes, B. (2010), "Experimental investigation of actively confined concrete using shape memory alloys", *Eng. Struct.*, **32**(3), 656-664.

Singh, M., Raj, A. and Singh, B. (2011), "Modified mohr-coulomb criterion for non-linear triaxial and polyaxial strength of intact rocks", *J. Rock Mech. Min. Sci.*, **48**(4), 546-555.

Smith, S.S., Willam, K.J., Gerstle, K.H. and Sture, S. (1989), "Concrete over the top, or: Is there life after peak?", *ACI Mater. J.*, **86**(5), 491-497.

Spoelstra, M.R. and Monti, G. (1999), "FRP-confined concrete model", *ASCE J. Compos. Constr.*, **3**(3), 143-150.

Tan, T.H. (2005), "Effects of triaxial stress on concrete", *Proceedings of the 30th Conference on Our World in Concrete*

and Structures, Singapore, August.
Teng, J.G., Huang, Y.L., Lam, L. and Ye, L.P. (2007), "Theoretical model for fiber reinforced polymer-confined concrete", *ASCE J. Compos. Constr.*, **11**(2), 201-210.
Vonk, R. (1992), "Softening of concrete loaded in compression", Ph. D. Dissertation, Eindhoven University of Technology, the Netherlands.
Vu, X.H., Malécot, Y., Daudeville, L. and Buzaud, E. (2009), "Effect of the water/cement ratio on concrete behavior under extreme loading", *J. Numer. Analy. Meth. Geomech.*, **33**(17), 1867-1888.
Willam, K.J. and Warnke, E.P. (1995), "Constitutive model for the triaxial behavior of concrete", *Proceedings of the 19th Seminar on Concrete Structure Subjected to Triaxial Stresses*, Bergamo, Italy.
Xiao, Q.G., Teng, J.G. and Yu, T. (2010), "Behavior and modeling of confined high-strength concrete. *ASCE J. Compos. Constr.*, **14**(3), 249-259.
Xie, J., Elwi, A.E. and MacGregor, J.G. (1995), "Mechanical properties of three high-strength concretes containing silica fume", *ACI Mater. J.*, **92**(2), 135-145.

CC